DOI: 10.1002/chem.201102944

Branched Mesoporous Mn_3O_4 Nanorods: Facile Synthesis and Catalysis in the Degradation of Methylene Blue

Zhongchao Bai,[a] Bo Sun,[a] Na Fan,[a] Zhicheng Ju,[b] Menghua Li,[a] Liqiang Xu,*[a] and Yitai Qian[a, b]

Abstract: Branched MnOOH nanorods with diameters in the range of 50–150 nm and lengths of up to tens of micrometers were prepared by using potassium permanganate ($KMnO_4$) and PEG 400 (PEG = polyethylene glycol) as starting materials through a simple hydrothermal process at 160 °C. After annealing at 300 °C under a N_2 atmosphere for 5 h, MnOOH nanorods became gradually dehydrated and transformed into mesoporous Mn_3O_4 nanorods with a slight size-shrinking. The as-obtained mesoporous Mn_3O_4 nanorods had an average surface area of 32.88 $m^2 g^{-1}$ and a mean pore size of 3.7 nm. Through tuning the experimental parameters, such as the annealing atmosphere and temperature, β-MnO_2, Mn_2O_3, Mn_3O_4, MnO, and Mn_5O_8 were selectively produced. Among these structures, mesoporous Mn_3O_4 nanorods were efficient for the catalytic degradation of methylene blue (MB) in the presence of H_2O_2 at 80 °C.

Keywords: manganese · methylene blue · mesoporous materials · nanostructures · porosity

Introduction

Mesoporous transition-metal oxides have attracted tremendous attention over the past decade, owing to their unique catalytic, electrochemical, magnetic, and adsorptive properties.[1–3] The traditional preparation methods for these mesoporous materials always involve the use of soft templates (typically surfactants, such as triblock copolymer F127, for mesoporous silica or carbon) or hard templates (such as mesoporous silica or anodic alumina, for other mesoporous materials).[4–11] However, soft-template methods usually lead to amorphous frameworks, and hard-template methods require complex procedures.[12–14] Moreover, the scarcity of suitable metallic precursors also limits the application of template methods to prepare most mesoporous transition-metal oxides. Therefore, it is still a great challenge to search for new synthesis methods for porous materials.

The thermal decomposition of hydroxide, carbonate, oxalate, and other metal salts is an effective strategy for synthesizing porous materials.[15–17] By using this method, pores are formed when gases (such as H_2O, CO_2, and CO) are released during the thermal decomposition of metallic salts. Compared with template methods, this technique does not require complex equipment or tedious post-processing (such as the removal of a template or selective etching in an appropriate solvent), which would introduce impurities and limit the applications of the mesoporous materials. Therefore, such a strategy is more promising than the template methods in industrial manufacturing.

Manganese oxides have been extensively studied because of their outstanding structural flexibility and their physical and chemical properties, such as their catalytic, electrochemical, magnetic, and adsorptive properties. Amongst all of the manganese oxides studied, Mn_3O_4 is unique owing to its mixed-valence state. Therefore, Mn_3O_4 has many excellent properties, including as a promising sensor material for detecting volatile organic compounds,[18] as an energy-storage material for anodes of lithium-ion batteries, and as an important catalyst in various oxidation and reduction reactions.[19–23] It is well-known that mesoporous materials are more effective than bulk materials when used as catalysts, adsorbents, and energy-storage materials. However, the synthesis of mesoporous Mn_3O_4 is still a great challenge because Mn_3O_4 is difficult to synthesize by direct template methods.[1]

Herein, mesoporous Mn_3O_4 nanorods were synthesized through the thermal decomposition of MnOOH nanorods at low temperatures under a nitrogen atmosphere. These mesoporous Mn_3O_4 nanorods were characterized by XRD, TEM,

[a] Z. Bai, B. Sun, Dr. N. Fan, M. Li, Prof. L. Xu, Prof. Y. Qian
Key Laboratory of Colloid and Interface Chemistry
Shandong University, Ministry of Education
and School of Chemistry and Chemical Engineering
Shandong University, Jinan 250100 (P. R. China)
Fax: (+86) 531-88366280
E-mail: xulq@sdu.edu.cn

[b] Dr. Z. Ju, Prof. Y. Qian
Hefei National Laboratory for Physical Science
at Microscale and Department of Chemistry
University of Science and Technology of China
Hefei, Anhui, 230026 (P. R. China)

Supporting information for this article, including the experimental conditions, XRD patterns, TEM images of the synthesized manganese oxides (β-MnO_2, Mn_2O_3, Mn_3O_4 without pores, MnO, and Mn_5O_8), electrochemical investigations, the cycle performance of the mesoporous Mn_3O_4 nanorods, and the TEM images of the products that were generated at different times during the formation of the branched nanorods, is available on the WWW under http://dx.doi.org/10.1002/chem.201102944.

SEM, and HRTEM. Besides these mesoporous Mn_3O_4 nanorods, β-MnO_2, MnO, and Mn_5O_8 nanorods were also selectively prepared from the thermal decomposition of MnOOH nanorods under different experiment conditions. The catalytic performances of these manganese-oxide nanorods were evaluated in the catalytic oxidation of methylene blue (MB).

Results and Discussion

The as-prepared MnOOH and Mn_3O_4 compounds were characterized by X-ray diffraction (Figure 1). In Figure 1a,

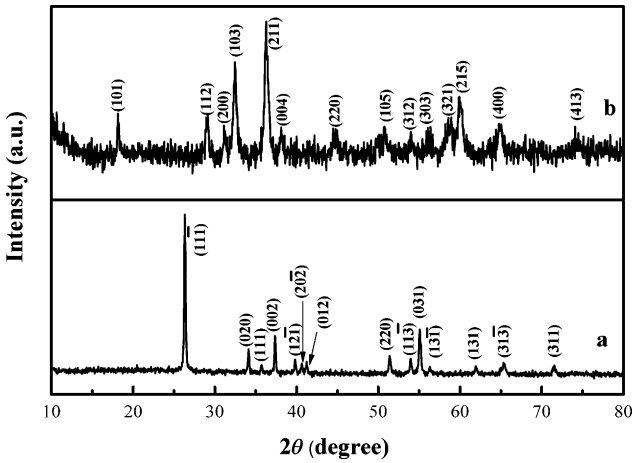

Figure 1. XRD patterns of a) MnOOH and b) mesoporous Mn_3O_4 nanorods.

all of the diffraction peaks corresponded to monoclinic MnOOH (space group $P2_1/c14$; JCPDS card no. 41-1379). This result was supported by the FTIR spectrum (Figure 2a). The peaks at 400–650 cm^{-1} were assigned to Mn–O vibrations, and the peaks at 1083, 1118, and 1155 cm^{-1} were attributed to the out-of-plane bending modes of γ-OH and the in-plane bending modes of δ-2-OH and δ-1-OH, respectively. This spectrum shows the representative bands of the γ-MnOOH phase.[24,25] In Figure 1b, all of the diffraction peaks of the product after calcination at 300°C were indexed to the hausmannite structure of Mn_3O_4 (space group $I4_1/amd$; JCPDS card no. 24-0734), which agreed with the standard values of bulk Mn_3O_4. In addition, the peaks were

Abstract in Chinese:

摘要 以高锰酸钾和聚乙二醇400为原料，通过简单的水热法在聚四氟乙烯为内衬的不锈钢反应釜中160 °C首先合成了直径为50~150 nm，长达几十微米的枝状MnOOH 纳米棒。经300 °C氮气气氛中退火5 h后，枝状MnOOH 纳米棒脱水并转化为尺寸更小的多孔Mn_3O_4枝状纳米棒，其比表面积为32.88 m^2g^{-1}，平均孔径约为3.7 nm。实验结果表明所得多孔的Mn_3O_4材料可在80°C，H_2O_2存在的条件下有效的催化降解亚甲基蓝；此外，通过实验参数的调整还可以实现β-MnO_2，Mn_2O_3, MnO和Mn_5O_8一维棒状材料的选择性合成。

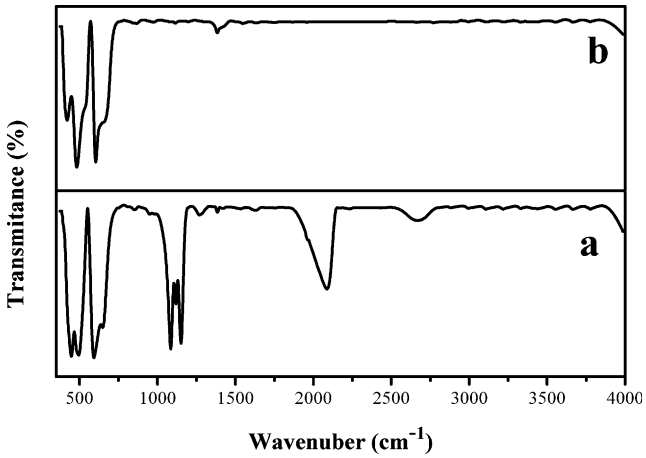

Figure 2. FTIR spectra of a) MnOOH and b) mesoporous Mn_3O_4 nanorods.

broad and weak, owing to the poor crystallinity or the small crystal domain in the product, which resulted from the low preparation temperature. The FTIR spectrum (Figure 2b) also confirmed that the sample was manganese oxide. The peaks centered at 417, 481, and 602 cm^{-1} were maintained in the FTIR spectrum, but the peaks owing to the O–H group disappeared, thus indicating its absence in the product. This result was in good agreement with the identification of the product as Mn_3O_4.

Figure 3 shows the field-emission SEM (FESEM) images of the as-obtained MnOOH and Mn_3O_4. Most of the MnOOH particles displayed typical rod-like shapes and smooth surfaces (Figure 3a, b). The diameters of these nanorods were in the range 50–150 nm and their lengths were up to tens of micrometers. Many nanorods grew on the surface

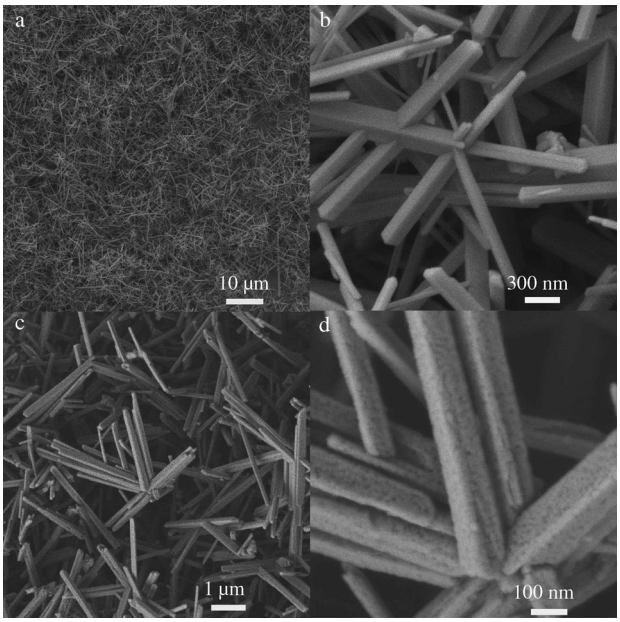

Figure 3. FESEM images of a) branched MnOOH nanorods and c) mesoporous Mn_3O_4 nanorods; b, d) magnified FESEM images of (a) and (c), respectively.

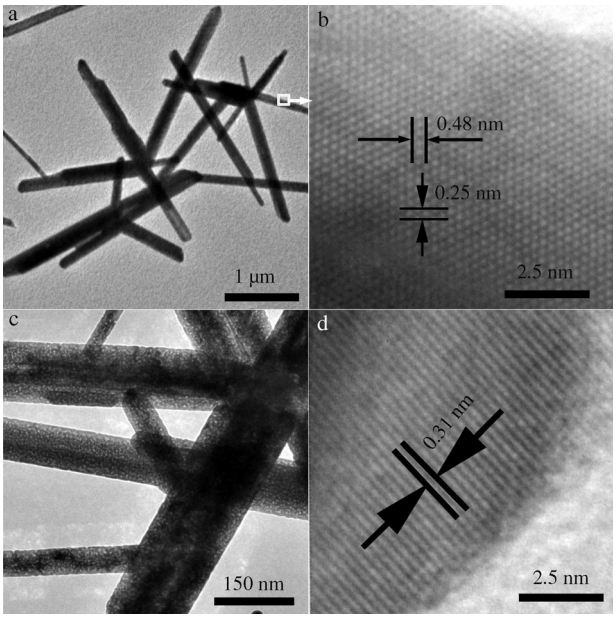

Figure 4. a) TEM image of branched MnOOH nanorods; b) HRTEM of branched MnOOH nanorods; c) TEM image of mesoporous Mn_3O_4; d) HRTEM of mesoporous Mn_3O_4 nanorods.

of the other nanorods, thereby producing branch-like trees. This branched rod-like feature was also observed by TEM (Figure 4a). The HRTEM image (Figure 4b) shows clear lattice fringes of 0.25 nm and 0.48 nm, which corresponded to the {111} and {110} crystal planes of MnOOH, respectively. The branched rod-like feature was also observed in the Mn_3O_4 particles after the calcination of the MnOOH nanorods at 300 °C (Figure 3c,d). However, the surface of the Mn_3O_4 nanorods became rough and some pore-like structures appeared on the surface, which was confirmed by pore-size measurements and TEM analysis. The diameter of these Mn_3O_4 nanorods was slightly smaller than before the calcination, which was attributed to a shrinkage caused by the decomposition of MnOOH. TEM analysis of the Mn_3O_4 nanorods also showed the existence of the pores ($d=2$–5 nm), which were distributed throughout the whole of the nanorods (based on the contrast difference; Figure 4c). A HRTEM image of a mesoporous Mn_3O_4 nanorod showed a distance between neighboring lattice fringes of about 0.31 nm, which was attributed to the {112} crystal plane of tetragonal Mn_3O_4 (Figure 4d).

The nitrogen-adsorption/desorption isotherms of MnOOH and Mn_3O_4 are shown in Figure 5. MnOOH exhibited an isotherm of type II (Figure 5a), which was the normal form of isotherms gained with a non-porous or macroporous adsorbent. The surface area was only 8.5 m^2g^{-1}. However, the Mn_3O_4 sample showed an isotherm of type IV (Figure 5b).[26] The hysteresis loops did not close at $P/P_0<1$ and such results are often ascribed to the aggregates of nanoparticles. The Mn_3O_4 sample had a high surface area of 32.88 m^2g^{-1}. The total pore volume was 0.053 m^3g^{-1}. The pore-size distribution (Figure 6), which was calculated by using (N_2) original density functional theory (DFT) assuming slit-pore geometry suggested micro- and mesoporosity. BJH desorption gave an average pore-width of 3.7 nm, which was in agreement with the TEM observations. This result was due to the conversion of MnOOH into Mn_3O_4 with a significant loss of oxygen and hydrogen, during which the pore-formation occurred. Therefore, the surface area of Mn_3O_4 was much larger than that of MnOOH.

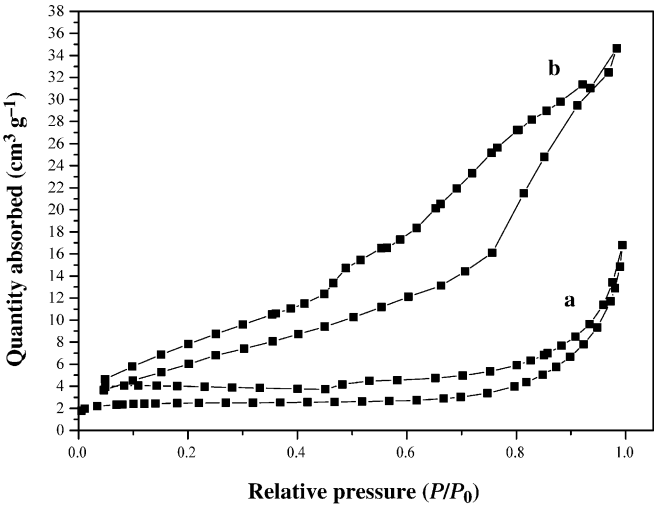

Figure 5. BET isotherm linear plots for a) MnOOH and b) Mn_3O_4.

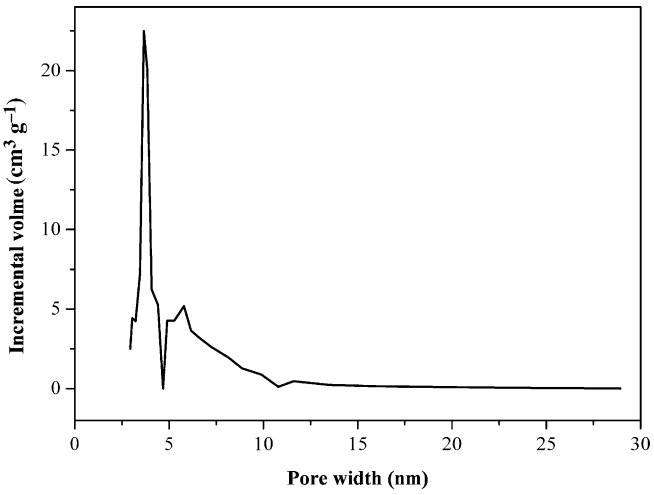

Figure 6. Pore-size distribution curve obtained for mesoporous Mn_3O_4.

A series of contrast experiments were carried out to investigate the effects of the reaction parameters on the mesoporous Mn_3O_4 nanorods. Because the mesoporous Mn_3O_4 nanorods were prepared by a hydrothermal reaction, followed by thermal annealing, these two processes were investigated separately. First, the effect of the reaction temperature on the hydrothermal reaction was investigated: If the temperature was below 120 °C, only nanoparticles were obtained. At 160 °C, branched MnOOH nanorods were produced. At 180 °C, coexistence of Mn_3O_4 nanoparticles with MnOOH was observed in the final products. Besides the reaction temperature, the reaction time also played an important role in the formation of branched MnOOH. The longer

the reaction time (up to 5 h), the larger the amount of branched MnOOH nanorods obtained; after 5 h, their yield remained almost unchanged. PEG 400 was one of the essential reagents for the formation of branched MnOOH nanorods. When PEG 400 was replaced by poly(4-vinylphenol) (PVP) or sodium dodecylbenzenesulfonate (SDBS), branched nanorods were not observed. We also investigated the formation of branched MnOOH nanorods. Nanoparticles were formed during the initial stages of the reaction (see the Supporting Information, Figure S4a) and then grew into coarse nanorods with increased reaction time (see the Supporting Information, Figure S4b). The coarse nanorods turned into smooth nanorods with small nanorods attached onto their surfaces (see the Supporting Information, Figure S4c). With further prolonged reaction time, the attached nanorods grew into branched nanorods (see the Supporting Information, Figure S4d). Based on these above experimental results, we considered that PEG 400 played a pivotal role in the formation of the MnOOH nanorods during the early stages of the reaction. As PEG 400 is a nonionic surfactant with uniform, ordered chain-structure and has multiple coordinating sites, it was easily adsorbed onto the surface of the metal-oxide colloid during the synthesis, thereby confining the colloid and facilitating the anisotropic growth of the 1D nanocrystals.[27,28,29] With a prolonged reaction time, the diameters and lengths of these nanorods increased notably. To reduce the total interfacial energy of the system, large amounts of these nanorods tended to aggregate and grow into branched structures. This self-assembly process was similar to that reported previously.[30] Finally, branched nanorods were obtained in high yields. To further study the effect of the PEG chain-length on the final product, comparative experiments were performed by substituting PEG (M_w= 400) with the same mass of PEG (M_w=200, 600, 800, 2000, and 20000). SEM images indicated that there was little difference among these products.

It is well-known that metal hydroxides can be converted into their corresponding oxides by thermal annealing. The annealing parameters (e.g., temperature, reaction time, and atmosphere) are critical for controlling the phase and morphology of the final products. Therefore, we studied the thermal-annealing behavior of MnOOH under air and nitrogen atmospheres, respectively. The TGA curves of MnOOH under N_2 and air atmospheres are shown in Figure 7a, b. First, MnOOH decomposed into β-MnO_2 (see the Supporting Information, Figures S1d and S2b) between 250 and 280 °C. Then, β-MnO_2 released oxygen and turned into Mn_2O_3 (see the Supporting Information, Figures S1a and S2c) between 550 and 600 °C. Finally, Mn_2O_3 released more oxygen and changed into Mn_3O_4 between 930 and 950 °C (see the Supporting Information, Figures S1b and S2e). The weight losses of the corresponding parts were 1.65%, 10.38%, and 13.1%, which were close to the theoretical values of 1.13%, 10.22%, and 13.25%, respectively (Figure 7b). This pattern is typical of the decomposition of MnOOH in air.[31] However, the TGA curve under a N_2 atmosphere was different. First, MnOOH decomposed into

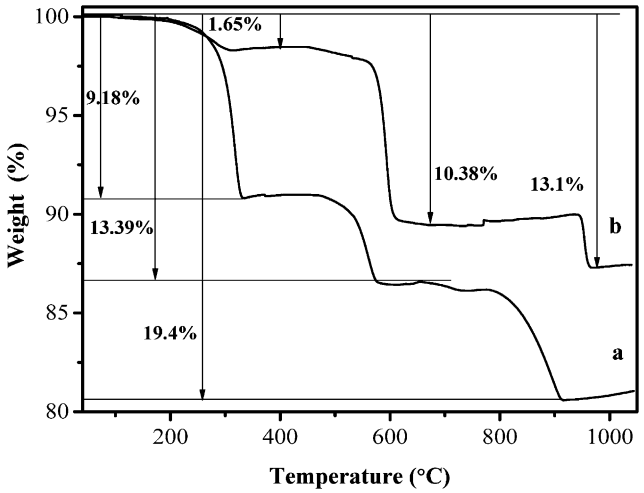

Figure 7. TGA curves of MnOOH nanorods under a) N_2 flow and b) air.

Mn_5O_8, then into Mn_3O_4, and finally into MnO (see the Supporting Information, Figures S1e and S2d). The weight-loss of every step was also consistent with the theoretical value. This process was the same as in most of the previous reports.[31,32] However, when MnOOH nanorods were annealed at 300 °C for 2 h under a nitrogen atmosphere, Mn_5O_8 nanorods were obtained (see the Supporting Information, Figures S1c and S2a). Mesoporous Mn_3O_4 nanorods were formed after 5 h. The latter process was not reflected in the TGA curve, presumably because the decomposition of MnOOH was a very slow process at low temperatures and the TGA test was a very fast heating process (heating rate: 10 °C min^{-1}). Therefore, some of the slow-decomposition process could not be detected in the TGA curve. To further investigate the decomposition behavior of MnOOH under a nitrogen atmosphere, a fine-TGA test was carried out at 300 °C (Figure 8). MnOOH gradually decomposed over 5 h at 300 °C under a N_2 atmosphere, and the weight loss was 13.2%, which agreed with the theoretical value of

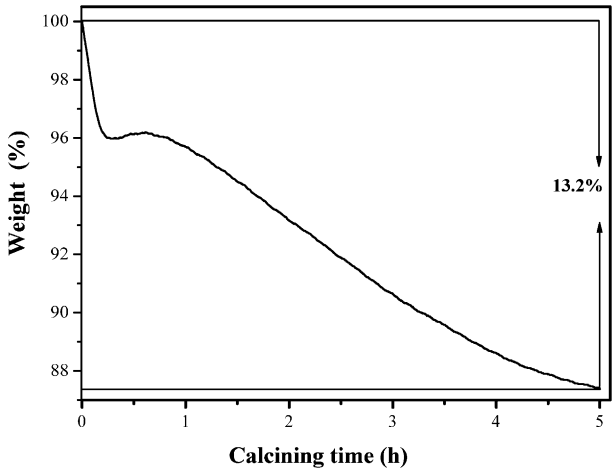

Figure 8. TGA curves of MnOOH at 300 °C for 5 h under a N_2 atmosphere.

13.25% for decomposition into Mn_3O_4. Therefore, the decomposition process of MnOOH at 300°C under a N_2 atmosphere can be represented as given in Equation (1):

$$MnOOH \rightarrow Mn_5O_8 \rightarrow Mn_3O_4 \quad (1)$$

First, MnOOH decomposed into Mn_5O_8 and then into Mn_3O_4 as the annealing time increased. Low synthesis temperatures did not destroy the pores that formed during the decomposition process. Therefore, the mesoporous Mn_3O_4 nanorods were obtained.

The as-obtained mesoporous Mn_3O_4 nanorods were used as a catalyst for waste-water treatment. MB, as a typical industrial pollutant, was chosen as a model to examine the catalytic performance of the mesoporous Mn_3O_4 nanorods. As the degradation of MB proceeds, the characteristic absorption of MB at 665 nm gradually weakens, which was why it was chosen for monitoring the catalytic process of mesoporous Mn_3O_4 nanorods. The catalytic performance of mesoporous Mn_3O_4 in the presence of H_2O_2 is shown in Figure 9. The initial spectrum showed four absorption peaks (245, 292, 614, and 664 nm), which originated from the molecular absorption of MB.[32] The intensities of these peaks quickly decreased within 10 min. The MB bands at 292 and 245 nm were covered by the strong absorption of hydrogen peroxide. As the reaction proceeded, the color of the solution slowly changed from dark blue to colorless. No obvious new band was observed in the spectrum (Figure 9), thereby suggesting the complete degradation of the MB molecules. The degradation efficiency of the MB molecules was calculated by $(I_0-I)/I_0$, where I_0 was the absorbance at 665 nm at $t=0$ and I was the absorbance at the same wavelength at a given reaction time. The degradation efficiency of the as-prepared mesoporous Mn_3O_4 nanorods was 95% after 1 h and 99.8% after 2 h (Figure 10d), which was slightly more-effective than the Mn_3O_4 nanorods (prepared herein; Figure 10c), Mn_3O_4 octahedra, and MnO_2 nanorods.[33–35] The good catalytic performance of the mesoporous Mn_3O_4 nanorods may have been due to the mesoporous (high surface area) and 1D structures (high surface-to-volume ratio). No obvious decolorization was observed without Mn_3O_4 or H_2O_2, even after 2 h (Figure 10a,b),[33] which indicated that the degradation of MB molecules was caused by H_2O_2-induced oxidation, catalyzed by Mn_3O_4.

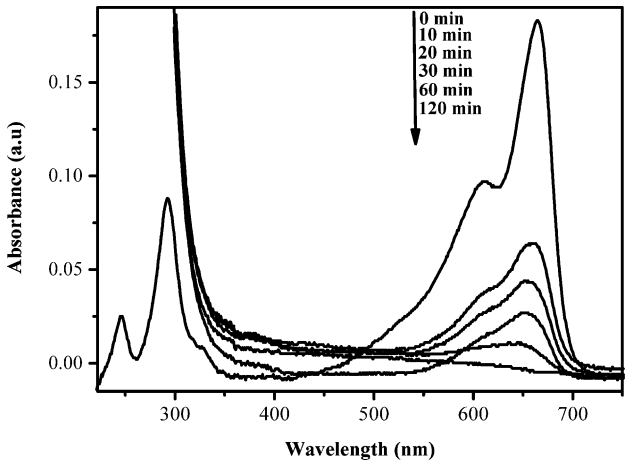

Figure 9. Absorption spectra of a mixture of of MB (100 mg L^{-1}, 50 mL), branched mesoporous Mn_3O_4 nanorods (0.01 g), and H_2O_2 (20 mL, 30 wt%) that was heated at 80°C for different time intervals of 0, 10, 20, 30, 60, and 120 min.

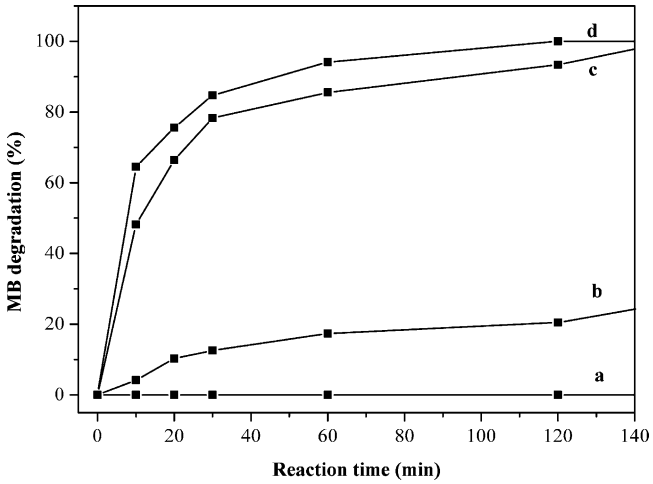

Figure 10. Time profiles of MB degradation: a) mesoporous Mn_3O_4 nanorods+MB, b) H_2O_2+MB, c) Mn_3O_4 nanorods without pores+MB+H_2O_2, and d) mesoporous Mn_3O_4 nanorods+MB+H_2O_2.

Our preliminary experiments have shown a relatively high energy-storage capacity of mesoporous Mn_3O_4 nanorods in lithium-ion batteries (560 mAhg^{-1} after 35 cycles at 50 mAg^{-1}; see the Supporting Information, Figure S3). This value is larger than those of Mn_3O_4 nanofibers (450–500 mAhg^{-1}) and MnO/C composites (200–300 mAhg^{-1}).[36,37] This result was ascribed to the mesoporous (high surface area that allowed the electrode and the electrolyte with sufficient contact area) and 1D structures (1D electron-transport pathways) of the mesoporous Mn_3O_4 nanorods.[38]

Conclusion

Branched MnOOH nanorods were successfully synthesized by using a simple and mild hydrothermal procedure. The anisotropic growth of MnOOH was attributed to the PEG-assisted oriented attachment of nanocrystalline material. Mesoporous Mn_3O_4 and other kinds of branched manganese oxides (β-MnO_2, Mn_2O_3, MnO, and Mn_5O_8.) were obtained as desired by performing the heat treatment of the MnOOH precursor under different temperatures and atmospheres. The as-obtained mesoporous Mn_3O_4 nanorods exhibited effective catalysis for oxidative decomposition of MB and high energy-storage capacity in lithium-ion batteries.

Experimental Section

Synthesis of mesoporous nanorods Mn_3O_4: All of the reagents were analytical grade and used without further purification. In a typical synthesis of branched MnOOH nanorods, PEG 400 (2 mL) and potassium permanganate ($KMnO_4$) (0.1 g) were mixed together and placed into a 60 mL Teflon cup. Distilled water was added up to 70% of the total volume under violent magnetic agitation. Next, the Teflon-lined autoclave was sealed tightly and was heated at 160°C for 5 h, before being allowed to cool to room temperature. The precipitates were collected by filtration, washed several times with distilled water and absolute EtOH, and finally dried at 60°C for 5 h. The as-prepared precipitate was calcined at 300°C under a N_2 atmosphere for 5 h to afford mesoporous Mn_3O_4 nanorods. For details of the synthesis other manganese oxides (β-MnO_2, Mn_2O_3, Mn_3O_4, MnO, and Mn_5O_8), see the Supporting Information, Table S1.

Catalytic oxidation reaction: The catalysis experiment was carried out in a 250 mL glass flask that contained an aqueous MB solution (100 mg L^{-1}, 50 mL), distilled water (50 mL), and mesoporous Mn_3O_4 nanorods (10 mg). After 30 wt% H_2O_2 solution (20 mL) was added, the mixture was heated to 80°C with continuous stirring. At given time intervals, 1 mL of the mixture was removed and quickly diluted with distilled water to 5 mL total volume prior to analysis.

Instruments: X-ray powder diffraction (XRD) patterns were obtained from a Bruker D8 advanced X-ray diffractometer that was equipped with graphite-monochromated $Cu_{K\alpha}$ radiation ($\lambda = 1.5418$ Å). Field-emission scanning electron microscopy (FESEM) images were taken with a JEOL JSM-7600F field-emission instrument. High-resolution TEM (HRTEM) images were recorded on a JEOL-2011 high-resolution transmission electron microscope at an acceleration voltage of 200 kV. FTIR spectra were measured on a Shimadzu FTIR-8400S spectrometer. Thermal gravimetric analysis (TGA) was carried out on a Mettler Toledo TGA/SDTA851 thermal analyzer apparatus under air and N_2 flows, respectively. Nitrogen-sorption measurements were performed on a Tristar II 3020 M gas sorptometer. Samples were degassed to 0.003 mm Hg for 12 h at 60°C. Specific surface areas were calculated by using the Brunauer–Emmett–Teller (BET) method, and pore sizes and volumes were estimated from pore-size distribution curves from the adsorption branches of the isotherms. Absorption spectra were measured with a TU-1901 UV/Vis spectrophotometer.

Acknowledgements

This work was supported by the 973 Project of China (No. 2011CB935901), the National Nature Science Found of China and the Academy of Sciences large apparatus United Fund (No. 11179043), the National Nature Science Fund of China (Nos. 91022033, 20971079, and 20871075), and the Independent Innovation Foundations of Shandong University (2009TS017, 2009 JC019, and yzc10092). The authors are grateful to Dr. Junling Duan for the UV spectroscopic data.

[1] F. Jiao, A. Harrison, A. H. Hill, P. G. Bruce, *Adv. Mater.* **2007**, *19*, 4063.
[2] E. S. Toberer, T. D. Schladt, R. Seshadri, *J. Am. Chem. Soc.* **2006**, *128*, 1462.
[3] Y. G. Li, B. Tan, Y. Y. Wu, *Nano Lett.* **2008**, *8*, 265.
[4] Y. P. Zhai, Y. Q. Dou, X. X. Liu, S. S. Park, C. S. Ha, D. Y. Zhao, *Carbon* **2011**, *49*, 545.
[5] B. Z. Tian, X. Y. Liu, B. Tu, C. Z. Yu, J. Fan, L. M. Wang, S. H. Xie, G. D. Stucky, D. Y. Zhao, *Nat. Mater.* **2003**, *2*, 159.
[6] S. R. Gajjela, K. Ananthanarayanan, C. Yap, M. Gratzelc, P. Balaya, *Energy Environ. Sci.* **2010**, *3*, 838.
[7] Y. Liu, W. W. Zhao, X. G. Zhang, *Electrochim. Acta* **2008**, *53*, 3296.
[8] C. L. Xu, Y. Q. Zhao, G. W. Yang, F. S. Lia, H. H. Li, *Chem. Commun.* **2009**, 7575.
[9] G. X. Wang, H. Liu, J. Horvat, B. Wang, S. Z. Qiao, J. Park, H. A. Highly, *Chem. Eur. J.* **2010**, *16*, 11020.
[10] F. Jiao, J. C. Jumas, M. Womes, A. V. Chadwick, A. Harrison, P. G. Bruce, *J. Am. Chem. Soc.* **2006**, *128*, 12905.
[11] J. Yang, J. J. Peng, R. X. Zou, F. Peng, H. J. Wang, H. Yu, J. Y. Lee, *Nanotechnol.* **2008**, *19*, 255603.
[12] C. C. Yu, X. P. Dong, L. L. Guo, J. T. Li, F. Qin, L. X. Zhang, J. L. Shi, D. S. Yan, *J. Phys. Chem. C.* **2008**, *112*, 13378.
[13] J. P. Xie, Q. B. Zhang, W. J. Zhou, J. Y. Lee, D. I. C. T. Wang, *Langmuir* **2009**, *25*, 6454.
[14] S. Pruneanu, L. Olenic, S. A. F. Al-Said, G. Borodi, A. Houlton, B. R. Horrocks, *J. Mater. Sci.* **2010**, *45*, 3151–3159.
[15] C. C. Yu, L. X. Zhang, J. L. Shi, J. J. Zhao, J. H. Gao, D. S. Yan, *Adv. Funct. Mater.* **2008**, *18*, 1544.
[16] L. P. Zhu, G. H. Liao, Y. Yang, H. M. Xiao, J. F. Wang, S. Y. Fu, *Nanoscale Res. Lett.* **2009**, *4*, 550.
[17] Z. H. Yang, W. X. Zhang, Q. Wang, X. M. Song, Y. T. Qian, *Chem. Phys. Lett.* **2006**, *418*, 46.
[18] L. C. Zhang, Q. Zhou, Z. H. Liu, X. D. Hou, Y. B. Li, L. Yi, *Chem. Mater.* **2009**, *21*, 5066.
[19] P. Li, C. Y. Nan, Z. Wei, J. Lu, Q. Peng, Y. D. Li, *Chem. Mater.* **2010**, *22*, 4232.
[20] H. L. Wang, L. F. Cui, Y. Yang, H. S. Casalongue, J. T. Robinson, Y. Y. Liang, Y. Cui, H. J. Dai, *J. Am. Chem. Soc.* **2010**, *132*, 13978.
[21] H. Einaga, S. Futamura, *J. Catal.* **2004**, *227*, 304.
[22] X. Q. Li, L. P. Zhou, J. Gao, H. Miao, H. Zhang, J. Xu, *Powder Technol.* **2009**, *190*, 324.
[23] W. M. Wang; Y. N. Yang, J. Y. Zhang, *Appl. Catal. A* **1995**, *133*, 81.
[24] P. K. Sharma, M. S. Whittingham, *Mater. Lett.* **2001**, *48*, 319.
[25] L. Hernan, J. Morales, J. L. Tirado, *Surf. Coat. Technol.* **1986**, *27*, 343.
[26] A. Vinu, P. D. Sawant, K. Ariga, M. Hartmann, S. B. Halligudi, *Microporous Mesoporous Mater.* **2005**, *80*, 195.
[27] Z. H. Wang, L. L. Wang, H. Wang, *Cryst. Growth Des.* **2008**, *8*, 4415.
[28] D. S. Zhang, H. X. Fu, L. Y. Shi, C. S. Pan, Q. Li, Y. L. Chu, W. J. Yu, *Inorg. Chem.* **2007**, *46*, 2446.
[29] Z. Q. Li, Y. J. Xiong, Y. Xie, *Inorg. Chem.* **2003**, *42*, 8105.
[30] Y. Zeng, T. Zhang, L. J. Wang, R. Wang, *J. Phys. Chem. C.* **2009**, *113*, 3442–3448.
[31] O. P. Ferreira, L. Otubo, R. Romano, O. L. Alves, *Cryst. Growth Des.* **2006**, *6*, 601.
[32] T. Gao, Norby. F. Krumeich, H. Okamoto, R. Nesper, H. Fjellvåg, *J. Phys. Chem. C.* **2010**, *114* , 922.
[33] P. Q. Zhang, Y. G. Zhan, B. X. Cai, C. C. Hao, J. Wang, C. X. Liu, Z. J. Meng, Z. L. Yin, Q. Y. Chen, *Nano Res.* **2010**, *3*, 235.
[34] W. X. Zhang, Z. G. Yang, X. Wang, Y. C. Zhang, X. G. Wen, S. H. Yang, *Catal. Commun.* **2006**, *7*, 408.
[35] Z. H. Yang, Y. C. Zhang, W. X. Zhang, X. Wang, Y. T. Qian, X. G. Wen, S. H. Yang, *J. Solid State Chem.* **2006**, *179*, 679.
[36] Q. Fan, M. S. Whittingham, *Electrochem. Solid-State Lett.* **2007**, *10*, A48.
[37] Q. Hao, L. Q. Xu, G. D. Li, Z. C. Ju, C. H. Sun, H. Y. Ma, Y. T. Qian, *J. Alloys Compd.* **2011**, *509*, 6217.
[38] F. Y. Cheng, H. B. Wang, Z. Q. Zhu, Y. Wang, T. R. Zhang, Z. L. Tao, J. Chen, *Energy Environ. Sci.* **2011**, *4*, 3668.

Received: September 19, 2011
Published online: March 13, 2012

